Gd, I-doped TiO$_2$ thin films coated on solid waste material: synthesis, characterization, and photocatalytic activity under UV or visible light irradiation

Siwei Deng[1,2] · **Jiang Yu**[1,2] · **Chun Yang**[3] · **Jiahua Chang**[1,2] · **Yizheng Wang**[1,2] ·
Ping Wang[1,2] · **Shiqian Xie**[1,2]

Abstract In this work, titanium dioxide thin films doped with different concentrations of gadolinium (Gd) and iodine (I) were synthesized using the sol–gel method and successfully coated on solid waste material (made in our lab) by dipping, resulting in the titanium dioxide thin-film-coated material (TiO$_2$M). Then, the doped titanium dioxide thin films were characterized by X-ray diffraction (XRD), SEM, and UV–Vis spectroscopy; the optimum coating cycle was evaluated by removal rates of COD and ammonia nitrogen in raw wastewater and secondary effluent. Moreover, the photocatalytic activity was determined by degradation efficiency of methyl orange. The results showed that TiO$_2$M had desirable reusability and the photocatalytic activity was attractive under ultraviolet light irradiation. Furthermore, it is found that the amount of dopant in TiO$_2$ was a key parameter in increasing the photoactivity. 1% Gd-doped TiO$_2$M exhibited the best photocatalytic activity for the degradation of methyl orange with the removal rate reaching 85.55%. The result was in good agreement with the observed smaller crystallite size and profitable crystal structure (anatase phase). Besides, the TiO$_2$M (0.8% Gd-doped TiO$_2$M, 1% Gd-doped TiO$_2$M, 10% I-doped TiO$_2$M, and 5% I–1% Gd-doped TiO$_2$M) with desirable photocatalytic activity at ultraviolet light irradiation was selected for the visible light photocatalytic experiments with taking methyl orange as the target pollutants. The results showed that all of them exhibited the similar photocatalytic activity after 7 h of sunlight irradiation (around 90% removal effect). In general, this research developed a very effective and environmentally friendly photocatalyst for pollutant degradation.

1 Introduction

At present, environmental problems caused by economic development have raised serious concerns over the need for renewable sources of clean energy, degradation of pollutants, and recycling of waste material [1]. TiO$_2$ with various morphologies, made by different methods, has been widely employed in photocatalytic degradation of pollutants, water splitting, solar cells, supercapacitors, biomedical devices, and lithium batteries due to their low-cost, good physical and chemical properties [2, 3]. However, there are several limitations to using powder TiO$_2$ in photocatalytic reactors of waste water as follows: (a) its powder form making it difficult the separation stage and (b) only exciting by ultraviolet (UV) light due to its large bandgap energy (anatase: 3.2 eV and rutile: 3.0 eV) [4, 5].

The research of TiO$_2$ immobilized on supports and modified by doping with metal, non-metal, and semiconductor to drive the visible light, prevent the recombination of electron/holes, and enhance utilization of solar energy is the focus of the current research to overcome these problems [6–9]. The doping materials include Fe, Cu, V, Mn, Zn, Ag, N, S, etc. and the carriers of TiO$_2$ include non-woven cloth, metal, glass, biochar, graphene, CNT$_S$, zeolites, silica, beehives, etc. [10–13]. In addition, TiO$_2$ doped with rare earth elements such as La, Ce, Er, Pr, Gd, Nd, Sm, etc. has received great interests, because the 4f-

✉ Jiang Yu
  yujianggz@163.com

1 College of Architecture and Environment, Sichuan University, Chengdu 610065, China

2 Institute of New Energy and Low Carbon Technology, Sichuan University, Chengdu 610065, China

3 College of Chemistry and Materials Science, Sichuan Normal University, Chengdu 610068, China

electrons provide new energy levels in the bandgap of TiO_2, leading to the observed red-shift absorption, and enhancing the photocatalytic efficiency under UV and visible light [14–16]. Xu et al. presented a comparative study on the photocatalytic efficiency of undoped and Ln-doped TiO_2 ($Ln^{3+} = La^{3+}$, Ce^{3+}, Er^{3+}, Pr^{3+}, Gd^{3+}, Nd^{3+}, and Sm^{3+}) and found that Gd-doped TiO_2 had the highest activity among all samples investigated [17]. Researches have been shown that Gd-doped TiO_2–NFs had nearly fivefold enhancement in the PC degradation [18] and further improved the rate of photocatalytic degradation of RhB [19]. On the other hand, some studies have found that iodine doping may result in superior photocatalytic activity compared to other non-metal dopants due to the close ionic radii of I^{5+} and Ti^{4+} [20–22] and the co-doping TiO_2 with nonmetals resulted in more significant bandgap narrowing compared to metal doping, leading to high photocatalytic efficiency under visible light irradiation [23–25]. From carriers' point of view, the cost of carriers of TiO_2, such as CNTS and graphene, is very expensive. Moreover, with the shortage of natural resources, many researches focused on the recycle of solid waste materials in recent years. However, until now, few studies were reported using solid waste materials as the carrier of TiO_2. Therefore, it might be promising and environmentally friendly to explore the photocatalytic activity of Gd-doped TiO_2, I-doped TiO_2, and co-doped TiO_2 immobilized on solid waste material under UV and visible light irradiation.

In this work, Gd-doped TiO_2, I-doped TiO_2, and Gd–I-co-doped TiO_2 thin films were made using the sol–gel method and were coated on solid waste material (made by our laboratory) by dipping. The best coating cycle was evaluated by degradation of COD and ammonia nitrogen in raw wastewater and secondary effluent, and the photocatalytic activity was determined by degradation of methyl orange. Meanwhile, the Gd-doped TiO_2M and I-doped TiO_2M were characterized by X-ray diffraction (XRD), scanning electron microscope (SEM), and UV–Vis spectroscopy.

2 Materials and methods

2.1 Materials

All of the chemical reagents used in this study were of analytical grade from Chengdu Long Glass Co. (Sichuan, China). The solid waste material was made with the construction waste (mainly for discarded ceramics and glass) as raw materials, and bentonite, diatomite as accessories. It was spherical with the characteristics of lightweight (520 kg/m^3), high strength (4.05 MPa), large specific surface area (5.01 m^2/g), and light transmittance.

2.2 Preparation of TiO_2 thin-film-coated solid waste material

TiO_2 thin films were synthesized by the sol–gel method using butyl titanate (titania precursor), ethyl alcohol absolute, trolamine, and distilled water with volume rate of 3:12:1:1. The trolamine was added dropwise with constant stirring for 20 min to ethyl alcohol absolute. Then, the butyl titanate was added to the mixture with constant stirring for 30 min. Finally, the distilled water was added to the solution with constant stirring for 3 h. The temperature was controlled at 25 °C in the whole process. The final solution was aged for 1 day leading to the formation of TiO_2 in the form of gel. The TiO_2 gel was coated on the solid waste material (made by our laboratory) by dipping and then calcined at 500 °C for 2 h to get the titanium dioxide thin-film-coated material (TiO_2M). We have explored the best annealing condition for TiO_2M, resulting that TiO_2M at 500 °C for 2 h exhibited the best proportion of anatase phase (78.76% anatase and 21.24% rutile).

To evaluate the best coating cycle, the undoped TiO_2M was added to the pending water for photocatalytic reaction under the ultraviolet light irradiation. Samples were collected before and after reaction (2 h) during the irradiation and centrifuged before analysis. The pending water was raw wastewater and secondary effluent from the sewage treatment plant in Chengdu City, Sichuan Province, China.

The solid waste material coating I-doped TiO_2M, Gd-doped TiO_2M, and I–Gd-co-doped TiO_2M was similar to undoped TiO_2M. The only difference was that the aforementioned distilled water was replaced by the corresponding solution of $Gd(NO_3)_3$, HIO_3, and both $Gd(NO_3)_3$ and HIO_3, respectively. The dopant concentration of Gd was 0.5, 0.8, 1.0, 1.2, 1.5, and 3%, respectively, named 0.5% Gd–TiO_2M, 0.8% Gd–TiO_2M, 1.0% Gd–TiO_2M, 1.2% Gd–TiO_2M, 1.5% Gd–TiO_2M, and 3% Gd–TiO_2M, respectively. The dopant concentration of I was 1, 5, and 10% named 1% I–TiO_2M, 5% I–TiO_2M, and 10% I–TiO_2M, respectively. The co-dopant concentration was 5% I and 1% Gd, named 5% I–1% Gd–TiO_2M.

2.3 Photocatalytic activity of the photocatalysts

The photocatalytic activity of the undoped TiO_2M and doped TiO_2M in the best coating cycle (5 times) was determined by degradation of methyl orange under ultraviolet light or visible light irradiation. The experiment of ultraviolet light was conducted in a photocatalytic reactor, which is a glass cylinder (500 mL) with an ultraviolet lamp from Philips Co. (15 W ultraviolet sterilization, with an emission spectrum of 350–400 nm, and λ_{max} at 370 nm) in the center (Fig. 1). The solution of methyl orange (100 mL) with a concentration of 20 mg/L and the
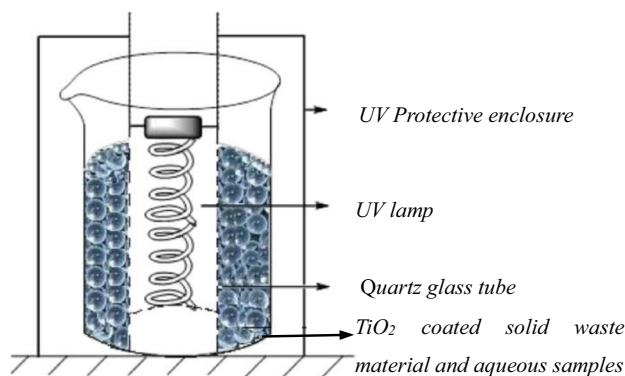
Fig. 1 Schematic of experimental apparatus

undoped TiO_2 and doped TiO_2 photocatalyst materials were added into the photocatalytic reactor. The solution was stirred and bubbled with atmospheric oxygen for 30 min in the dark to allow equilibration of the system, so that the loss of methyl orange due to adsorption could be taken into account. Then, irradiations were carried out by turning on the ultraviolet tube (15 W) for 2 h. Samples (10 mL) were collected before and after the irradiation. The desirable-doped TiO_2M in ultraviolet light was selected for the visible light photocatalytic experiments, which were conducted in light sun for 7 h. Samples (10 mL) were collected at regular intervals (1 h) during the irradiation. The methyl orange was monitored using UV–Vis spectrophotometer (Alpha-1506) at 464 nm.

2.4 Characterization of the photocatalysts

The structural characterization of undoped TiO_2 and doped TiO_2M photocatalyst material was performed by XRD (Shimadzu D/max-A) with Cu Ka radiations ($k = 1.5418$ Å) operated at voltage of 30 kV and a current of 15 mA. The morphology of the particles was examined using SEM (Hitachi S-5000 FEG) operated at a voltage of 20 kV. The UV–Vis spectra were recorded at room temperature in the range of 200–800 nm using a Shimadzu UV–Vis spectrophotometer (UV-3600) with $BaSO_4$ as the reference.

3 Results and discussion

3.1 Optimizing the coating cycle of TiO₂ thin films

To obtain the best coating cycle of TiO_2 thin film on the solid waste material, the removal rates of COD and ammonia nitrogen in raw wastewater and secondary effluent were investigated. Figure 2 shows comparison of the photocatalytic activity for COD and ammonia nitrogen removal rates obtained from 1, 2, 3, 4, 5, and 6 time coating

cycle samples. These results evidenced that with the increasing coating cycle of undoped TiO_2, photocatalytic activity increased both for COD and for ammonia nitrogen removal in raw wastewater and secondary effluent.

As we know, the photocatalytic activity mainly occurs on the surface layer of TiO_2 thin film, and it is observed that the dispersion and uniformity of TiO_2 thin-film surface layer were similar under six-coated times and five-coated times in the experiment, which resulted in the photocatalytic rate was almost the same of the one obtained for five times at the two conditions. Thus, the sample chosen to investigate the characteristics and the photocatalytic ability working with visible light and ultraviolet light for methyl orange was optimized as five time coating cycles.

Furthermore, the coated materials were reused four times successively to examine the durability and reusability of the TiO_2M towards the removal of COD and ammonia nitrogen under ultraviolet light irradiation (Fig. 3). Each test lasted for 2 h. The results showed that photocatalytic activity decreased gradually with the increase of use frequency. However, after reusing four times, the material still kept good photocatalytic activity compared with the first use.

3.2 XRD and SEM analysis

The XRD spectra of the undoped and doped TiO_2 with different concentrations of Gd and I are shown in Figs. 4 and 5. There was no peak of I^- and Gd^{3+}. The reasons might be the formation of the bonds Ti–O–Gd and Ti–O–I or there was no atomic reunion because of the low concentration of $Gd(NO_3)_3$ and HIO_3.

Table 1 shows the crystallite size, the lattice distortion, and the crystal structure of the crystallites in the XRD peak (101). The average anatase crystallite sizes of doped and undoped TiO_2 thin films were determined by the Debye Scherer formula:

$$D = \frac{K\lambda}{\beta \cos \theta} \tag{1}$$

where D is the crystallite size, K is the shape factor, λ is the wavelength, β is the diffraction angle, and θ is the full-width at half-maximum.

The lattice distortion of the doped and undoped TiO_2 thin films was determined by the formula:

$$\varepsilon = \frac{\beta}{4tg\theta} \tag{2}$$

where ε is the lattice distortion, β is the diffraction angle, and θ is the full-width at half-maximum.

The percentage (X_A) of the anatase phase can be estimated from the respective intensities of peaks using the following equation:
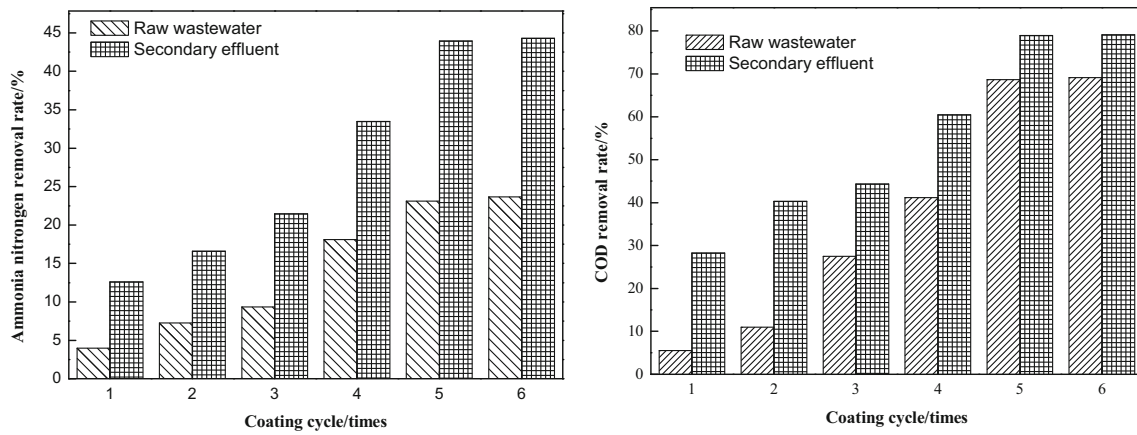
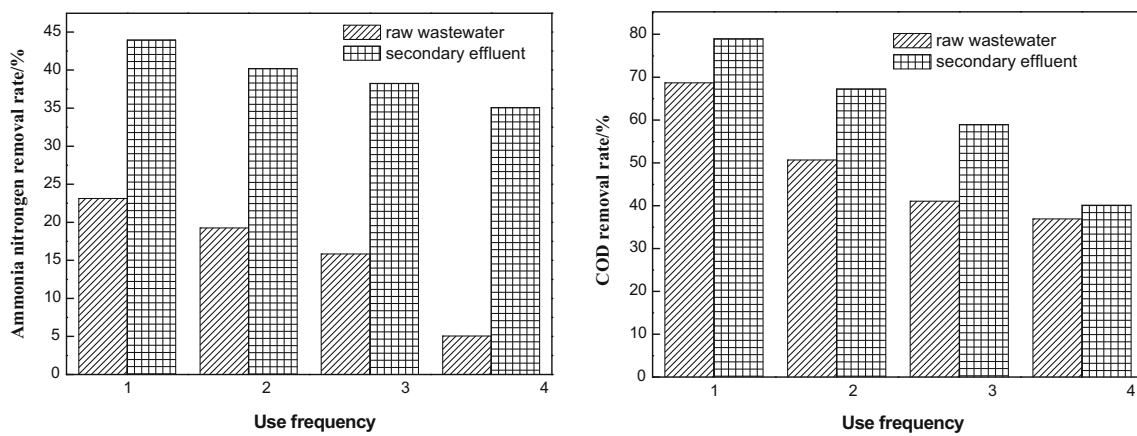**Fig. 2** COD and ammonia nitrogen removal rate under different coating cycles

Fig. 3 COD and ammonia nitrogen removal rate under different use frequencies
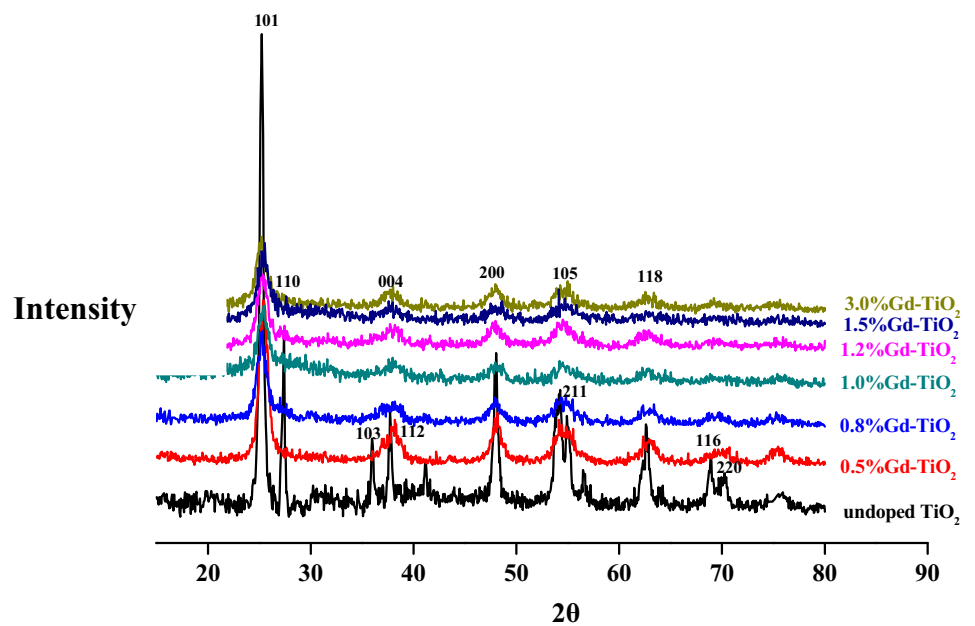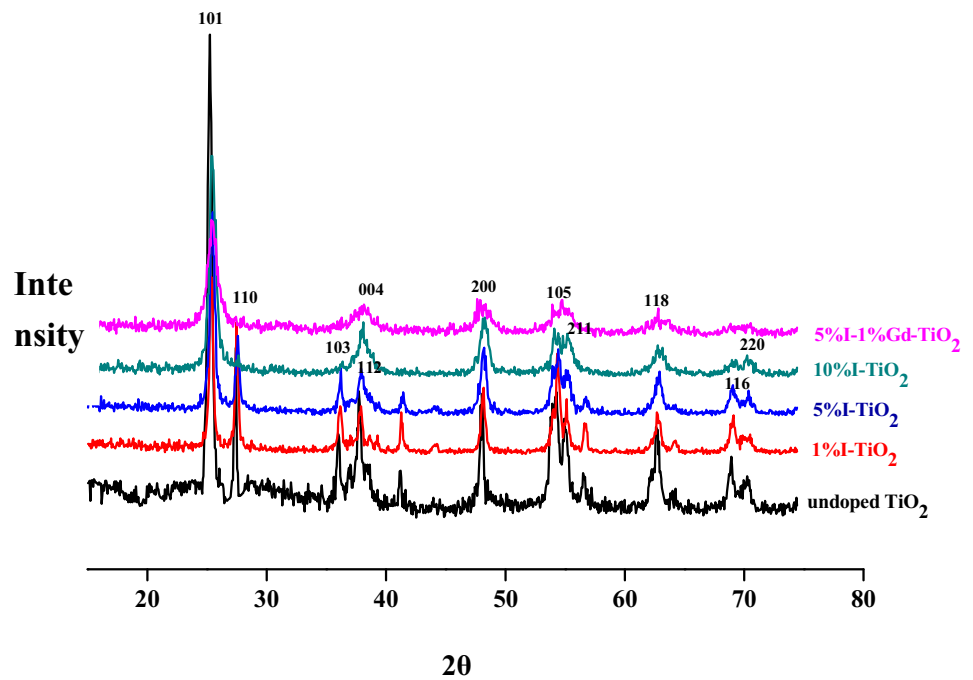
Fig. 4 XRD spectra of Gd-doped TiO$_2$

Fig. 5 XRD spectra of I-doped TiO₂

Table 1 XRD crystallographic data of undoped TiO₂ and doped TiO₂

Photocatalysts	Crystallite size D (nm)	Lattice distortion/ε	Crystal structure	
			Anatase phase (%)	Rutile phase (%)
Undoped TiO₂	21.82	0.412	77	23
0.5% Gd–TiO₂	10.30	0.869	100	0
0.8% Gd–TiO₂	10.82	0.829	100	0
1% Gd–TiO₂	9.34	0.960	100	0
1.2% Gd–TiO₂	10.82	0.829	100	0
1.5% Gd–TiO₂	11.10	0.810	100	0
3% Gd–TiO₂	12.43	0.715	100	0
1% I–TiO₂	23.48	0.381	58	42
5% I–TiO₂	22.31	0.399	75	25
10% I–TiO₂	14.35	0.623	100	0
5% I–1% Gd–TiO₂	11.54	0.775	100	0

$$X_A = \frac{100}{(1 + I_R/I_A)} \tag{3}$$

where I_A represents the intensity of the anatase peak at $2\theta = 25.25°$ and I_R represents the one of the peak rutiles at $2\theta = 27.4°$.

It could be seen from Table 1 that the crystallite size was found to decrease first, then to increase. The lattice distortion was found to increase first, then to decrease with the increase of dopant concentration of Gd (all better than the undoped TiO₂). The 1% Gd-doped TiO₂ had the optimal crystallite size and lattice distortion. The lattice distortion caused by the doping was in agreement with the experimental results,

where different dopings could cause different particle sizes [26–28] and dopants could favor the formation of smaller particles [29]. Susmita Paul found that the crystallite size was calculated to be 7.8 nm for pristine (0.00 mol) and 5.9, 5.45, and 5.42 nm for 0.03, 0.05, and 0.07 mol of Gd, respectively [30]. Because of the moderately large size incongruity with Ti⁴⁺ (0.68 Å), Gd³⁺ (0.94 Å) ions are not expected to inhabit sites in the lattice of TiO₂. They possibly stay on the particle surface and on the grain boundaries and produce a strain in those regions [31].

Moreover, all Gd-doped TiO₂ and 5 I–1% Gd-co-doped TiO₂ particles showed the 100% anatase phase and the

percentage of the anatase phase was found to increase along with the increase in dopant concentration of iodine. Cheng [14] found that Gd doping accelerates the anatase to rutile phase transformation at 1273 K for 2 h, which was different from this research. It might be the reason that the percentage of the rutile phase increased with increasing annealing temperature [32]. As Yang reported, Gd-, N-doped TiO_2, and Gd/N co-doped TiO_2 were all in anatase phase [33].

However, an interesting finding in our study was that the crystallite size of the 1% I-doped TiO_2 and 5% I-doped TiO_2 was slightly larger (23.48 and 22.31 nm, respectively) than that of undoped one (21.82 nm) and the percentage of anatase phase was lower (Table 1), indicating that iodine had opposite effect on the growth rate of anatase, the crystallite size, and the lattice distortion when the dopant concentration of I was low. This interesting phenomenon was also observed by Andreia Molea et al. [21]. There could be a critical crystallite size in process of phase transformation between anatase phase and rutile phase, which was in good agreement with the crystallite size and lattice distortion results in this study.

The structural characterizations of thin-film-coated material (TiO_2M) were carried out via scanning electron microscopy. The morphology of undoped and doped TiO_2 particles with Gd and I is presented in Fig. 6, respectively. As could be seen from Fig. 6a–d, the thin films of 10% I–TiO_2M, 1% Gd–TiO_2M, and 5% I + 1% Gd–TiO_2M were better and relatively few of them are reunited compared to undoped TiO_2M and the 1% Gd–TiO_2M and 5% I + 1% Gd–TiO_2M surface dispersion degree and uniform were better than 10% I–TiO_2M.

3.3 UV–Vis absorption spectra

The UV–Vis absorption spectra of the undoped TiO_2 and doped TiO_2 with different dopant concentrations of Gd and I were studied and the spectra are shown in Fig. 7, respectively. The bandgap energies of the undoped and doped TiO_2 particles with the obtained wavelength from UV–Vis absorption spectra were calculated by the following equation:

$$\text{Bandgap (eV)} = \frac{1240}{\text{wavelength (nm)}}. \tag{4}$$

The bandgap energies of the undoped and doped TiO_2 with different dopant concentrations of Gd and I are listed in Table 2. As expected, dopants of Gd and I into TiO_2 lattice were found to shift the fundamental absorption edge towards the longer wavelength, which decreased the bandgap energy [34]. However, in case of Gd-doped TiO_2, the bandgap energy was found to decrease first and then increased with the increasing dopant concentration. Moreover, the bandgap energy was found to increase with

the increasing dopant concentration of iodine. This might be due to the deposition of the excessive Gd and iodine on the photocatalyst which covered the surface of TiO_2 and reduced the effective surface area for absorbing light [35]. In other words, there was an optimum dopant concentration for Gd and I. The optimal dopant concentration of Gd was 1% in this work, which was in good agreement with the XRD results.

3.4 Photocatalytic activity under ultraviolet light irradiation

To compare the photocatalytic activity of undoped TiO_2M and doped TiO_2M, the degradation of methyl orange under ultraviolet light irradiation was carried out, and the results are shown in Fig. 8. As could be seen, the photocatalytic activity of Gd-doped TiO_2M increases first, and then decreases with the increasing concentration of Gd (all higher than undoped TiO_2M) and the 1% Gd-doped TiO_2M showed the optimal photocatalytic activity (85.55%). The reason might be that it might act as a recombination center, rather than facilitating electron–hole separation, resulting in decreased photocatalytic activity when the doping content was excessively high [13]. The photocatalytic activity of I-doped TiO_2M was found to increase with the increasing concentration of iodine, but 1% I-doped TiO_2M and 5% I-doped TiO_2M were lower than undoped TiO_2M. In addition, the similar research showed that the 15% I–TiO_2 sample may not be superior to 10% I–TiO_2M [24]. Furthermore, the 1% Gd–5% I-co-doped TiO_2M was superior to the 5% I-doped TiO_2M, which meant that the best dopant concentration of Gd and iodine was 1 and 10% with the highest photocatalytic activity for the degradation of methyl orange (85.55 and 77.83%, respectively), which was in good agreement with the XRD and UV–Vis results.

Moreover, the difference in the photocatalytic activity could be ascribed much to the crystallite size and crystal structure, which has the similar trend with different dopants (Table 2). It is known that the photocatalytic activity of TiO_2 was influenced by specific surface area, phase, and morphologies [36]. Anatase as a metastable phase exhibits the most activity in photocatalysis and the most stable rutile phase shows less activity or no activity at all [37]. Furthermore, dopant with too high concentration may form charge recombination centers and/or shield the surface of TiO_2 from light irradiation. The bandgap analysis (Table 2) showed that 1% Gd-doped TiO_2M and 10% I-doped TiO_2M samples had very close bandgap energies (3.047 and 3.39 eV, respectively), and the photocatalytic activity was 85.55 and 77.03%, respectively. It meant that the photocatalytic activity increased with the decrease of the energy bandgap, which was similar to the results found by other researchers [37].
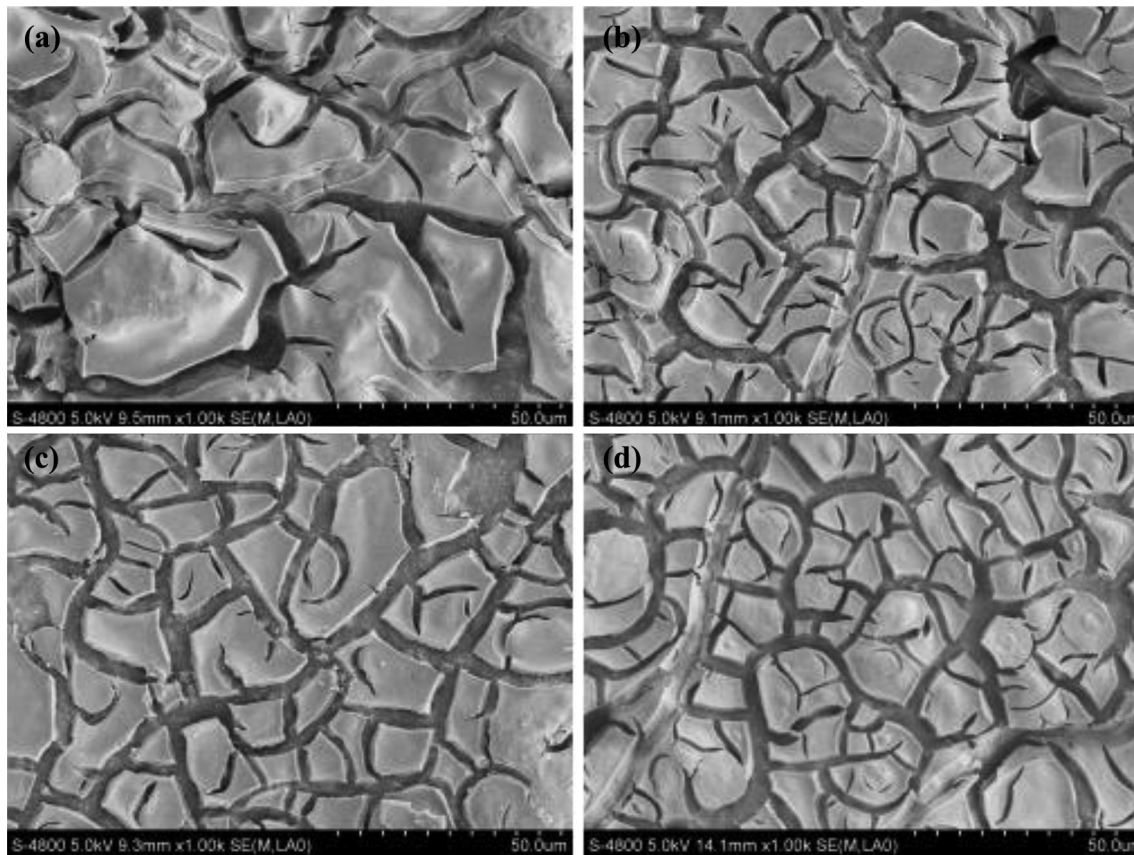
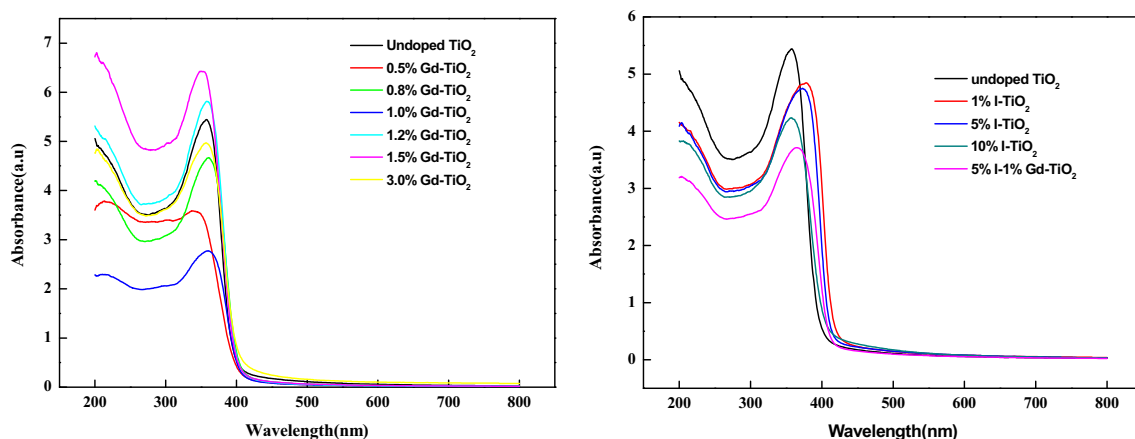**Fig. 6** SEM images of **a** undoped TiO$_2$M, **b** 10% I–TiO$_2$M, **c** 1% Gd–TiO$_2$M, **d** 5% I + 1% Gd–TiO$_2$M

Fig. 7 Ultraviolet–visible light absorption spectra of undoped TiO$_2$, Gd–TiO$_2$, and I–TiO$_2$

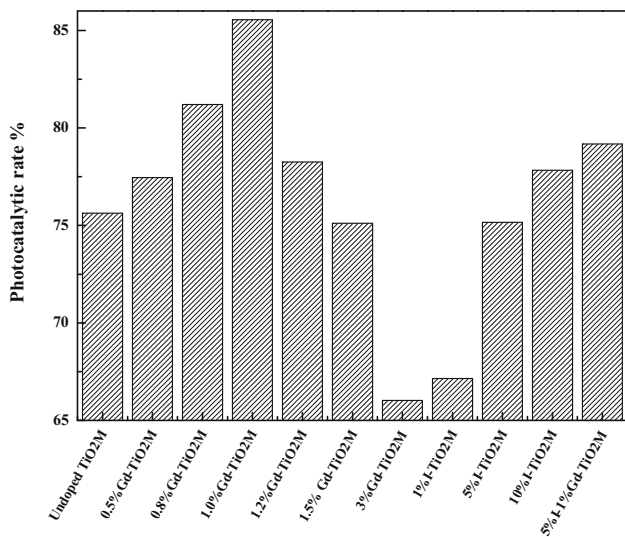### 3.5 Photocatalytic activity under visible light (sunlight) irradiation

TiO$_2$M with desirable photocatalytic activity at ultraviolet light irradiation (0.8% Gd-doped TiO$_2$M, 1% Gd-doped TiO$_2$M, 10% I-doped TiO$_2$M, and 5% I–1% Gd-doped TiO$_2$M) were selected for the visible light photocatalytic experiments with methyl orange as the target pollutants.

The experiment was conducted in sunlight for 7 h. Samples (10 mL) were collected at regular intervals (1 h) during the irradiation, and the results are shown in Fig. 9.

As can be seen, there was no obvious degradation of methyl orange in undoped TiO$_2$M under sunlight irradiation. However, the doped TiO$_2$M showed much better photocatalytic activity after 7 h irradiation, and 0.8% Gd-doped TiO$_2$M, 1% Gd-doped TiO$_2$M, 10% I-doped TiO$_2$M,

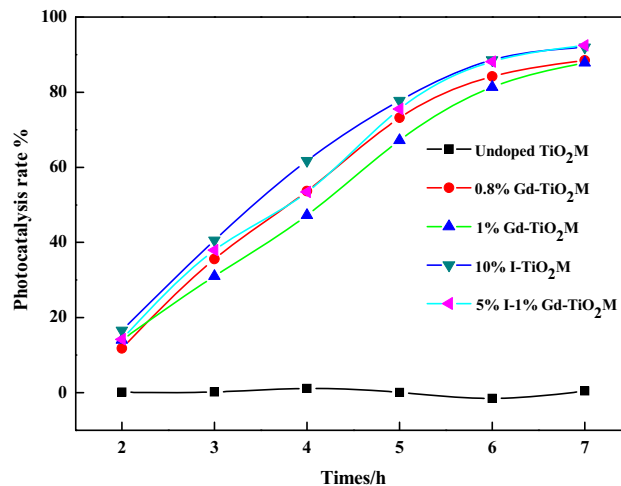**Table 2** Absorption threshold and bandgap of undoped TiO_2 and doped TiO_2

Photocatalysts	Wavelength (nm)	Bandgap (eV)
Undoped TiO_2	397	3.123
0.5% Gd–TiO_2	401	3.092
0.8% Gd–TiO_2	404	3.069
1% Gd–TiO_2	407	3.047
1.2% Gd–TiO_2	399	3.108
1.5% Gd–TiO_2	399	3.108
3% Gd–TiO_2	398	3.109
1% I–TiO_2	417	2.974
5% I–TiO_2	413	3.002
10% I–TiO_2	408	3.039
5% I–1% Gd–TiO_2	411	3.017

Fig. 9 Photocatalysis efficiency of undoped TiO_2, Gd–TiO_2, and I–TiO_2 under sunlight irradiation

reusability in the study. Using the SEM, UV, and XRD methods, it is found that Gd, I doping could reduce the crystallite size, increase the lattice distortion, and furtherly affect the phase, thus could increase the photocatalytic activity under ultraviolet light irradiation, and it is observed that the 1% Gd-doped TiO_2M had the best crystallite size, lattice distortion, 100% anatase phase, and the best photocatalytic activity (85.55%) for methyl orange within 2 h under ultraviolet light irradiation. However, there was an opposite effect on the growth rate of anatase, the crystallite size, and the lattice distortion when the doping concentration of I was very low.

In the process of experiment, it is found that Gd, I doping could extend the absorption spectra to the visible light region, also resulting in high photocatalytic activity under visible light irradiation. it is observed that a series of doped TiO_2M including 0.8% Gd-doped TiO_2M, 1% Gd-doped TiO_2M, 10% I-doped TiO_2M, and 5% I–1% Gd-doped TiO_2M showed much better photocatalytic activity after 7 h visible light irradiation compared to undoped TiO_2. Therefore, the TiO_2M photocatalyst could be considered a promising material for the application for the removal of pollutants in aqueous solution specially on organic pollutants.

Fig. 8 Photocatalysis efficiency of undoped TiO_2, Gd–TiO_2, and I–TiO_2 under UV irradiation

and 5% I–1% Gd-doped TiO_2M showed the similar photocatalytic activity for methyl orange degradation under sunlight irradiation (88.42, 87.83, 91.97, and 92.48%, respectively). The results could be related to its bandgap in Table 2, which meant that the doped TiO_2M enhanced the utilization of visible light.

4 Conclusions

The undoped TiO_2 and doped TiO_2 thin films synthesized by sol–gel method were coated on the solid waste material (made by our laboratory) by dipping successfully, then calcined at 500 °C for 2 h to get the titanium dioxide thin-film-coated material (TiO_2M) which showed the ideal reuse

References

1. N.V. Boltakova, G.R. Faseeva, R.R. Kabirov, R.M. Nafikov, Y.A. Zakharov, Waste Manag. **60**, 230 (2017)

2. Y. Zhang, Z.L. Jiang, J.Y. Huang, L.Y. Lim, W.L. Li, J.Y. Deng, D.G. Gong, Y.X. Tang, Y.K. La, Z. Chen, RSC Adv. **5**, 79479 (2015)
3. D. Pathar, R.K. Bedi, D. Kaur, Optoelectron. Adv. M. **5**, 657 (2010)
4. H. Tang, H. Berger, P.E. Schmid, F. Lévy, G. Burri, Solid State Commun. **9**, 847 (1993)
5. M.E. Borges, T. Herna'ndez, P. Esparza, Clean Technol. Environ. Policy **16**, 431 (2014)
6. N. Rahimi, R.A. Pax, E.M. Gray, Prog. Solid State Chem. **44**, 86 (2016)
7. M.Z. Ge, C.Y. Cao, J.Y. Huang, S.H. Li, S.N. Zhang, S. Deng, Q.S. Li, K.Q. Zhang, Y.K. Lai, Nanotechnol. Rev. **5**, 75 (2016)
8. M.Z. Ge, Q.S. Li, C.Y. Cao, J.Y. Huang, S.H. Li, S.G. Zhang, Z. Chen, K.Q. Zhang, S.S. Al-Deyab, Y.K. Lai, Adv. Sci. **4**, 1600152 (2017)
9. M.E. Borges, M. Sierra, E. Cuevas, R.D. García, P. Esparza, Sol. Energy **135**, 527 (2016)
10. D. Pathak, R.K. Bedi, D. Kaur, R. Kumar, J. Chalcogenied Lett. **8**, 213 (2011)
11. W. Zhang, B.P. Jia, Q. Wang, D. Dionysiou, J. Nanopart. Res. **17**, 211 (2015)
12. J.X. Lowa, B. Chenga, J.G. Yua, Appl. Surf. Sci. **392**, 658 (2017)
13. M.Z. Ge, C.Y. Cao, J.Y. Huang, S.H. Li, Z. Chen, K.Q. Zhang, S.S. Al-Deyabd, Y.K. Lai, J. Mater. Chem. **4**, 6772 (2016)
14. X.Q. Cheng, C.Y. Ma, X.Y. Yi, F. Yuan, Y. Xie, J.M. Hu, B.C. Hu, Q.Y. Zhang, Thin Solid Films **615**, 13 (2016)
15. K.P. Priyanka, V.R. Revathy, P. Rosmin, B. Thrivedu, K.M. Elsa, J. Nimmymol, K.M. Balakrishna, T. Varghese, Mater. Caract. **113**, 144 (2016)
16. D.F. Sun, K. Wang, Z.J. Xu, R.X. Li, J. Rare Earth **33**, 491 (2015)
17. A.W. Xu, Y. Gao, H.Q. Liu, J. Catal. **207**, 151 (2002)
18. J. Choi, P. Sudhagar, P. Lakshmipathiraj, J.W. Lee, A. Devadoss, S. Lee, T. Song, S. Hong, S. Eito, C. Terashima, T.H. Han, J.K. Kang, A. Fujishima, Y.S. Kang, U. Paik, RSC Adv. **4**, 11750 (2014)
19. J. Zhang, W.C. Wua, S. Yan, G. Chu, S.L. Zhao, X. Wang, C. Li, Appl. Surf. Sci. **344**, 249 (2015)
20. N. Bouazza, M. Ouzzine, M.A. Lillo-Ródenas, D. Eder, A. Linares-Solano, Appl. Catal. B Environ. **92**, 377 (2009)
21. A. Molea, V. Popescu, N.A. Rowson, Powder Technol. **230**, 203 (2012)
22. M.C. Long, W.M. Cai, Z.P. Wang, G.Z. Liu, Chem. Phys. Lett. **429**, 71 (2006)
23. Q.Y. Zhanga, Y. Li, A. Erik, G.J. Marija, H.L. Li, Appl. Catal. A **400**, 195 (2011)
24. J. Li, Q. Zhang, L. Zeng, D. He, Appl. Phys. **122**, 51 (2016)
25. D.D. Liu, Z.S. Wu, F. Tian, B.C. Ye, Y.B. Tong, J. Alloy Compd. **676**, 489 (2016)
26. B. Yang, M.D. Li, H. Zhang, A.Z. Yu, J.M. Lin, J.M. Zhao, S.P. Lir, Adv. Mater. Res. **1010**, 211 (2014)
27. B. Yang, Z.P. Zhu, Y. Zhou, C.J. Xia, Sci. Conf. Proc. **1**, 243 (2009)
28. Y. Zhou, K.L. Huang, Z.P. Zhu, B. Yang, H.Y. Qiu, Y. Gu, T. Liu, Cent. South Univ. **39**(4), 677 (2008)
29. K.X. Song, J.H. Zhou, J.C. Bao, Y.Y. Feng, Am. Ceram. Soc. **91**, 1369 (2008)
30. S. Paul, B. Choudhury, A. Choudhury, J. Alloy Compd. **601**, 201 (2014)
31. N.D. AbazovicB, M.B. Radoicic, T.D. Savic, I.A. Jankovic, M.I. Čomor, Dig. J. Nanomater. Biostruct. **8**, 871 (2013)
32. X.Y. Deng, Q.L. Ma, Y.Q. Cui, X.W. Cheng, Q.F. Cheng, Appl. Surf. Sci. **419**, 409 (2017)
33. B. Yang, M.D. Li, H. Zhang, A.Z. Yu, J.M. Lin, J.M. Zhao, S.P. Li, Adv. Mat. Res. **1010–1012**, 211 (2014)
34. V. Stengl, S. Bakardjieva, J. Phys. Chem. C **114**, 19308 (2010)
35. L.G. Devi, N. Murthy, Catal. Lett. **125**, 320 (2008)
36. Y.K. Lai, J.Y. Huang, Z.Q. Cui, M.Z. Ge, K.Q. Zhang, Z. Chen, L.F. Chi, Small **12**, 2203 (2016)
37. Q.Y. Zhanga, Y. Li, E.A. Ackerman, M.G. Josifovska, H.L. Li, Appl. Catal. A-Gen. **400**, 195 (2011)